MDPI

Article

Structural Evolution of Bulk Silver during Cold Rolling and Annealing

Zheda Ning [1], Qunshou Wang [2], Dong Zhao [2], Wenli Pei [2] and Ming Wen [1],*

1   State Key Laboratory of Advanced Technologies for Comprehensive Utilization of Platinum Metals, Kunming Institute of Precious Metals, Kunming 650106, China
2   School of Materials Science and Engineering, Northeastern University, Shenyang 110819, China
*   Correspondence: wen@ipm.com.cn; Tel.: +86-871-6832-9849

Abstract: Sputtering target is commonly used in semiconductor manufacturing for the preparation of thin films. Cold rolling and annealing treatment of bulk Ag is the routine process to prepare Ag sputtering target. In this paper, the microstructure evolution of Ag after cold rolling and annealing treatment was studied, and the results showed that annealing temperature affects the recrystallized structure of Ag and that 600 °C/1 h treatment can achieve complete recrystallization. At the same time, the texture evolution was also observed and discussed.

Keywords: silver; cold rolling; annealing; texture; microstructure; recrystallization

1. Introduction

Research interests in nanostructured materials such as thin films and nanoparticles have increased due to their excellent physical and chemical properties. Magnetron sputtering is one of the key technologies for the preparation of thin films/nanoparticles since it has many advantages such as high speed of deposition, low temperature, low damnification, repetition and stability. Because Ag has the highest reflectance in the visible region and the lowest resistivity among all metals, the application of Ag thin films/nanoparticles is very versatile. It can be used for building energy conservation [1,2], optoelectronics [3,4], microelectronics [5], solar cells [6,7], biomedicine [8,9], etc.

The sputtering target is the key consumable used in the magnetron sputtering process, and its microstructure has significant influence on the structure and properties of sputtering films. The regular process for the preparation of Ag targets is melting, plastic deformation and heat treatment. Nowadays, severe plastic deformation (SPD) is used for the production of ultrafine-grained (UFG) structure metal and alloys with high strength. SPD methods to prepare UFG metals included equal channel angular pressing (ECAP), high pressure torsion (HPT) and cumulative rolling bonding (ARB) [10–12]. Although there have been many studies on the SPD and microstructure characterization of Ag, the sample size is usually very small. However, the weight of an Ag ingot for the preparation of the Ag target is usually 10~20 kg. Due to the excellent ductility of Ag and the weight of the Ag target, the appropriate way to process the Ag target is by the melting, cold rolling and annealing treatment. Cold rolling of Ag reduced its thickness by more than 95% and subsequent annealing between 873 and 1073 K yielded the following recrystallization textures: {011}<011>, {011}<211> and {236}<385> [13–15]. Zhang et al. found that a strong {011}<211> recrystallization brass texture formed for Ag after cold rolling with 98% thickness reduction and two steps of annealing treatment at 423 K and 973 K [16]. In addition, after recrystallization annealing treatment, the rolling texture was transformed into annealing texture [17–20]. However, the formation and evolution of the annealing texture were affected by many factors such as deformation conditions and annealing temperature. In situ tension and synchrotron radiation X-ray diffraction were used, and they confirmed that grain growth, grain shrinking, twining, etc. occurred during the elastic

and plastic deformation of nanocrystalline Ag [21]. By now, there have been a few studies on the preparation process of Ag targets since the bulk size and the expensive price of Ag. Therefore, in the present work, the microstructure evolution of bulk Ag after the cold rolling and annealing treatment were studied, which could shed light on the preparation of the Ag target.

2. Materials and Methods

Silver ingots of 99.99 wt% purity and a weight of 15 Kg were induction melted in vacuum to get a rectangle ingot of $250 \times 120 \times 55$ mm. After hot rolling with a thickness reduction of 45%, a silver sheet with a thickness of about 30 mm was obtained. Subsequently, the silver sheet was cold rolled with pass deformation of 15% thickness reduction until the final thickness was 5 mm. Then the sheet was cut into several pieces using Electric Discharge Machining (EDM) and annealed at 300, 400, 500 and 600 °C for 1 h, respectively. Both rolling surface and longitudinal section samples of $10 \times 5 \times 5$ mm were cut by EDM for microstructure characterization. The metallography was conducted by using a Smart proof 5 confocal microscope (Zeiss, Oberkochen, Germany). The etching solution for metallography was a 1:1 solution which was mixed by nitric acid and hydrogen peroxide. The Vickers hardness (HV) of the samples was measured with the help of a digital micro-hardness tester (Tai Ming, Shanghai, China) with a load of 200 g and a dwell time of 10 s. In order to get the hardness distribution of Ag with depth from the rolling plane surface, at least six indents of similar depth were measured and the average calculated. The texture tests were performed by a Philips x-pert PRO X-ray diffractometer (Rigaku Corporation, Tokyo, Japan) with a copper target, and the experimental parameters were as follows: the tube voltage of 35 KV, the tube current of 40 mA, the light source of 5 mm parallel light, and a large window for the receiving slit. The α was between 0 and 70°, and β was between 0 and 360° with a step size of 5°. The analysis and measurement of texture was conducted by using the Orientation Distribution Function (ODF). ODFs were plotted in the format of iso-intensity contour lines with constant φ_2 sections with $\Delta \varphi_2$ equaled 5°.

3. Results

Figure 1 is an optical micrograph of Ag with the rolling plane. For Ag in the cold rolled state (Figure 1a), it can be seen that grains were not uniform, and grain boundaries were difficult to distinguish after the large plastic deformation during cold rolling (83.33% thickness reduction). After annealed at 300 °C (Figure 1b), although some area remained unchanged as compared with Figure 1a, recrystallization occurred in some other areas where the grain boundaries became sharp. As the annealing temperature increased to 400 °C (Figure 1c), more grains underwent recrystallization, and the grain size was more uniform when compared with Figure 1b. The grain boundaries became sharper; annealing twins also appeared when the temperature reached 500 °C (Figure 1d), and there were also some small grains distributed among the big grains suggesting they were still in the progress of recrystallization. For Ag annealed at 600 °C, it can be seen that the grains size was uniform, and almost all the grain boundaries were sharp suggesting the further progress of recrystallization. The mean grain size of Ag which annealed at 600 °C was 44.9 μm.
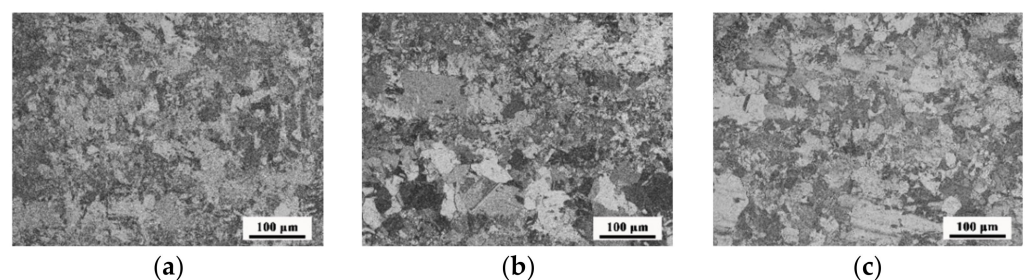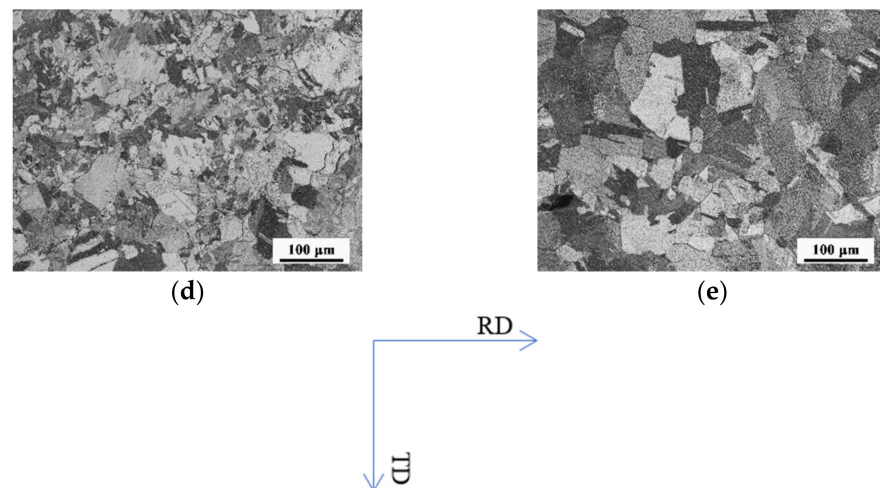

(**a**)　　　　　　　　(**b**)　　　　　　　　(**c**)

Figure 1. *Cont.*

Figure 1. Optical micrograph of Ag with the rolling plane: cold rolled (**a**) and following annealing at 300 °C (**b**), 400 °C (**c**), 500 °C (**d**), 600 °C (**e**), respectively (TD: Transverse direction, RD: Rolling direction).

In order to further observe the microstructure of Ag, the longitudinal section of Ag was also observed. Figure 2 is the optical micrograph of Ag with the longitudinal section. The microstructure evolution was almost the same with the rolling plane. Firstly, the diffused deformed grain structure was formed after cold rolling; then, with the increasing of the annealing temperature, recrystallization occurred in some local areas and then it spread in the whole Ag sheet, and recrystallization phenomena were more obvious at 600 °C with uniform grain structure and annealing twins also appearing in some grains (Figure 2a–e).
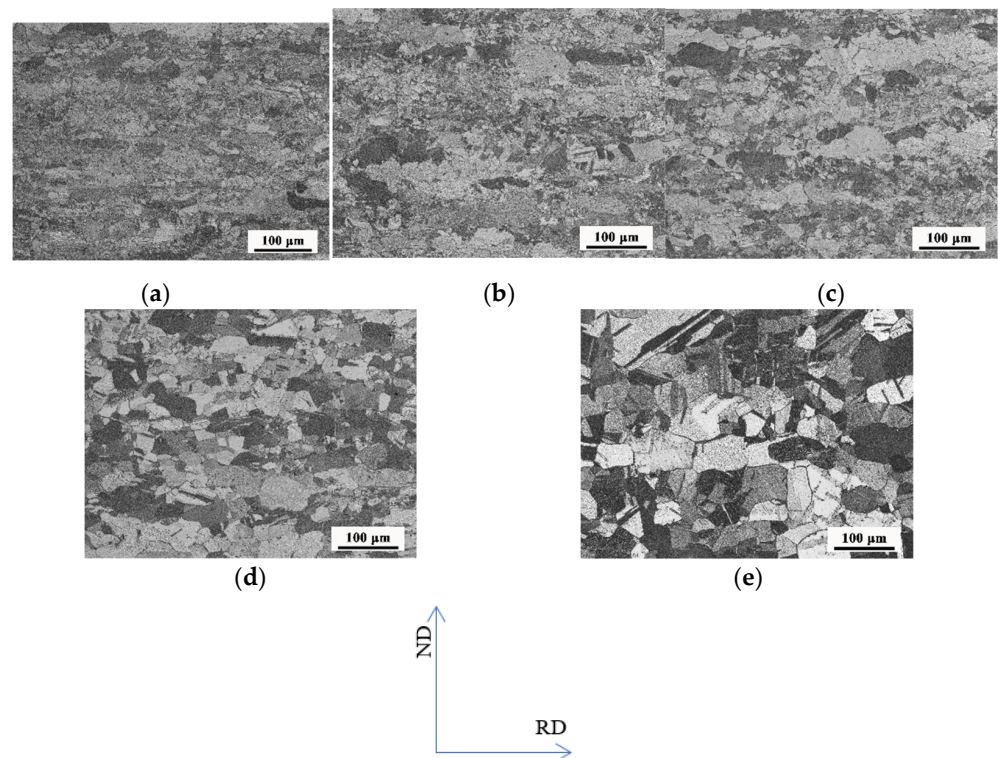

Figure 2. Optical micrograph of Ag with the longitudinal section: cold rolled (**a**) and following annealing at 300 °C (**b**), 400 °C (**c**), 500 °C (**d**), 600 °C (**e**), respectively (ND: Normal direction, RD: Rolling direction).

Figure 3 shows the hardness distribution of Ag with depth from the rolling plane surface (longitudinal section). At first, it can be seen that the hardness of Ag in the cold rolling state was the highest, and the hardness decreased with the increasing of annealing temperature. Secondly, for Ag in the cold rolling and annealed at 600 °C state, it can be seen that the hardness distribution along thickness was the most uniform, and the standard deviation of hardness was also the smallest among all the five samples. It was understandable since from Figure 2, due to the ongoing recrystallization between 300 and 500 °C, the grains sizes were inhomogeneous, which induced fluctuated hardness along thickness. On the contrary, for Ag in the cold rolling and annealed at 600 °C state, almost all the grains were equiaxed and exhibited approximately equal size. Thus, it can be inferred that annealing at 600 °C for 1 h was a suitable recrystallization treatment for the present cold rolled Ag.
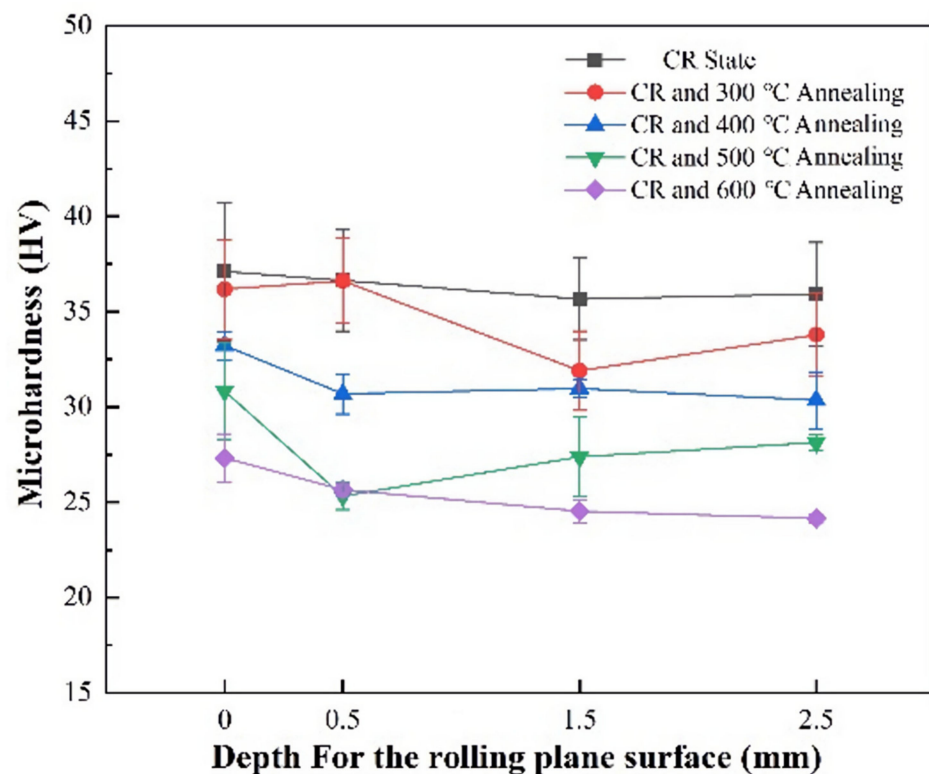

Figure 3. The hardness distribution of Ag with depth from the rolling plane surface.

Figure 4 shows the ODF of cold rolled Ag sheets. After large plastic deformation, it can be seen that the deformation texture was distributed near the {110} planes, which was mainly Goss orientation {110}<100>, and this was a typical fcc rolling texture.

Figure 5 shows the ODFs of Ag cold rolled and following annealing at 300~600 °C. It can be seen that after the annealing treatment, the Goss orientation was very weak, and {210}<001> orientation appeared, which means that the grain orientation shifted from the {110} plane to the {210} plane within the recrystallization process. The η orientation was presented in all of the cold rolling and the following annealing samples, while the intensity of η orientation was more obvious in the sample annealed at 300 °C than the other annealed at higher temperature (Figure 5a). When the annealing temperature increased to 400 °C, the {110}<110> orientation appeared (Figure 5b). At the same time, the {111}<112> orientation was found in all samples except that annealed at 400 °C (Figure 5c,d). It was also observed that a fringe of {001}<110> orientation existed in samples annealed at 300~500 °C, while it transformed into α orientation at the same site when the annealing temperature increased to 600 °C.
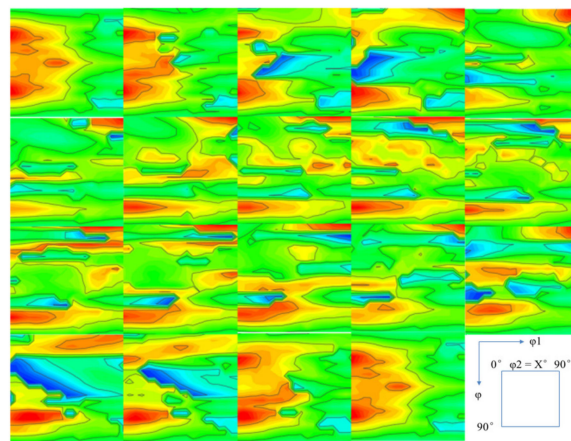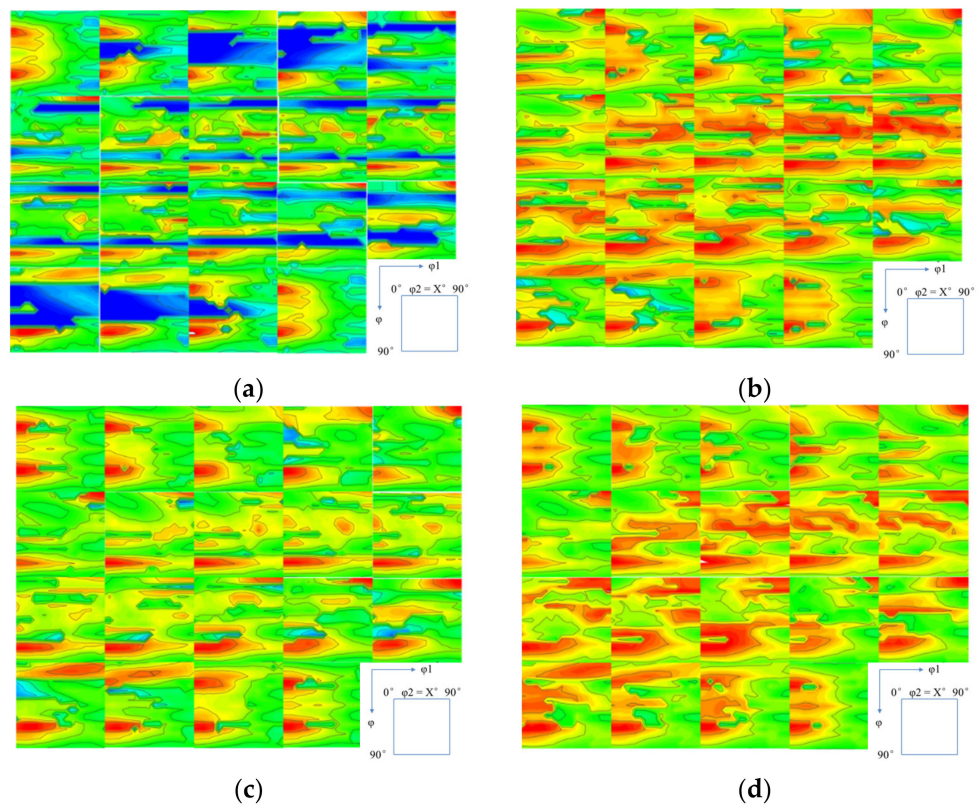
Figure 4. The ODF of cold rolled Ag sheets.

(**a**)

(**b**)

(**c**)

(**d**)

Figure 5. The ODFs of Ag sheets cold rolled and followed annealing at 300 °C (**a**), 400 °C (**b**), 500 °C (**c**), 600 °C (**d**), respectively.

4. Discussion

Usually, the deformed microstructure was composed by elongated grains along the rolling direction as with the increasing of deformation especially during cold rolling with deformation larger than 80% [22]. However, in the present study, the Ag sheet in cold rolling state with deformation of 83.33% did not show obvious elongated grain structure (Figure 2a). Ag has a very low stacking fault energy (SFE) of ~16 mJ/m^2, and thus, the annihilation of dislocations was hindered by their high degree of dissociation into partials which made the saturation dislocation density very high after severe plastic deformation [23]. These phenomena may affect the stability of the deformed microstructure of Ag. For example, Gubicza et al. found that the grain size increased from 250 nm to 1 μm for Ag, immediately, with 8 ECAP passes which were preserved for four months at room temperature [10]. In the present study, the deformation was enough to create a lot of

defects such as dislocations in cold rolled Ag sheet; dynamic recovery/recrystallization occurred and then disrupted the deformed grain structure. As with the increasing of annealing temperature, recovery and recrystallization occurred consequently and achieved well recrystallization at 600 °C (Figure 2b–d). The hardness distribution of Ag with depth from the rolling plane surface also showed that the hardness was more uniform in Ag with cold rolling and further annealing at 600 °C than the Ag with cold rolling and further annealed between 300 and 500 °C suggesting the uniform microstructure of the prior sample. Therefore, it can be concluded that 600 °C is a suitable temperature for the annealing treatment. Recrystallization begins in the zones with the highest stored energy, and the driving force for the growth of new grains is the difference in the stored energy, i.e., in the dislocation density [24]. In our research, as for the Ag with low SFE and large deformation, recrystallization began in some place where the dislocation density achieves some critical value, these dislocations annihilated and rearranged into ordered array and formed subgrain boundaries. Subgrain boundaries with higher dislocation density which had a large orientation difference on both sides, it was easy to migrate and gradually become the large angle boundaries during annealing treatment. And the migration of large angle boundaries further induced grains growth.

The cold rolled texture of Ag sheet obtained by relatively lower reductions in thickness was typical Brass-type rolling texture, and it converted to {0,4,11}<100> when rolling reduction in thickness increased to 98% [16].The annealing temperature changed the texture of Ag after cold rolling and following annealing treatment. It can be seen that after annealing treatment, the Goss orientation shifted to η orientation, {110}<110> orientation, {111}<112> orientation, and α orientation within 300~600 °C annealing temperature range (Figure 5). Besides the migration of grain boundaries, twinning was also played a role for the texture evolution with annealing temperature. It can be seen that annealing twins also appeared when the temperature between 500 and 600 °C (Figure 1d,e and Figure 2d,e). The texture of the fully recrystallized materials was formed by twinning and grain growth and created all the new orientations presented in the recrystallized microstructure [24]. The twinning and grain growth evolution during recrystallization still requires further investigation.

5. Conclusions

(1) During the cold rolling of bulk Ag sheet, the grains did not align along the rolling direction suggested. The microstructure underwent dynamic recovery/recrystallization due to the high defect density during the rolling process.

(2) The following annealing treatment after cold rolling showed that as with the increasing of annealing temperature, recovery and recrystallization occurred in Ag sheet, and annealing at 600 °C for 1 h was a suitable recrystallization treatment for present cold rolled Ag.

(3) The cold rolled Ag had mainly Goss orientation, and the deformation texture of Ag was affected by the deformation. After the annealing treatment, the Goss orientation shifted to η orientation, {110}<110> orientation, {111}<112> orientation, and α orientation with the increasing of temperature of 300~600 °C.

Informed Consent Statement: Not applicable.

Data Availability Statement: Data presented in this study may be requested from the corresponding authors.

Conflicts of Interest: The authors declare no conflict of interest.

References

1. Chiu, P.K.; Lee, C.T.; Chiang, D.; Cho, W.H.; Hsiao, C.N.; Chen, Y.Y.; Huang, B.M.; Yang, J.R. Conductive and transparent multilayer films for low-temperature $TiO_2/Ag/SiO_2$ electrodes by E-beam evaporation with IAD. *Nanoscale Res. Lett.* **2014**, *9*, 35. [CrossRef]
2. Cuce, E.; Cuce, P.M. Vacuum glazing for highly insulating windows: Recent developments and future prospects. *Renew. Sustain. Energy Rev.* **2016**, *54*, 1345–1357. [CrossRef]
3. Ho, S.M. A Review on Thin Films on Indium Tin Oxide Coated Glass Substrate. *Asian J. Chem.* **2016**, *28*, 469–472. [CrossRef]
4. Bao, S.Y.; Deng, X.; Mao, F.; Zhong, N.; Yue, F.Y.; Sun, L.; Xiang, P.H.; Duan, C.G. Ultra-flat ITO films on mica for high temperature transparent flexible electrodes. *Ceram. Int.* **2020**, *46*, 2268–2272. [CrossRef]
5. Shakiba, M.; Kosarian, A.; Farshidi, E. Effects of processing parameters on crystalline structure and optoelectronic behavior of DC sputtered ITO thin film. *J. Mater. Sci. Mater. Electron.* **2016**, *28*, 787–797. [CrossRef]
6. Wang, H.; Tang, C.; Shi, Q.; Wei, M.; Su, Y.; Lin, S.; Dai, M. Influence of Ag incorporation on the structural, optical and electrical properties of ITO/Ag/ITO multilayers for inorganic all-solid-state electrochromic devices. *Ceram. Int.* **2021**, *47*, 7666–7673. [CrossRef]
7. Yuan, Z.S.; Wu, C.C.; Tzou, W.C.; Yang, C.F.; Chen, Y.H. Investigation of high transparent and conductivity of IGZO/Ag/IGZO sandwich structures deposited by sputtering method. *Vacuum* **2019**, *165*, 305–310. [CrossRef]
8. Alias, R.; Mahmoodian, R.; Genasan, K.; Vellasamy, K.M.; Hamdi Abd Shukor, M.; Kamarul, T. Mechanical, antibacterial, and biocompatibility mechanism of PVD grown silver-tantalum-oxide-based nanostructured thin film on stainless steel 316L for surgical applications. *Mater. Sci. Eng. C Mater. Biol. Appl.* **2020**, *107*, 110304. [CrossRef]
9. Najafi, A.; Khoeini, M.; Khalaj, G.; Sahebgharan, A. Synthesis of silver nanoparticles from electronic scrap by chemical reduction. *Mater. Res. Express* **2021**, *8*, 125009. [CrossRef]
10. Gubicza, J.; Chinh, N.Q.; Lábár, J.L.; Tichy, G.; Hegedűs, Z.; Xu, C.; Langdon, T.G. Stability of microstructure in silver processed by severe plastic deformation. *Int. J. Mater. Res.* **2009**, *6*, 884–887. [CrossRef]
11. Balogh, L.; Ungár, T.; Zhao, Y.; Zhu, Y.T.; Horita, Z.; Xu, C.; Langdon, T.G. Influence of stacking-fault energy on microstructural characteristics of ultrafine-grain copper and copper–zinc alloys. *Acta Mater.* **2008**, *56*, 809–820. [CrossRef]
12. Zhao, Y.H.; Horita, Z.; Langdon, T.G.; Zhu, Y.T. Evolution of defect structures during cold rolling of ultrafine-grained Cu and Cu–Zn alloys: Influence of stacking fault energy. *Mater. Sci. Eng. A* **2008**, *474*, 342–347. [CrossRef]
13. Doi, T.; Mori, M.; Shimohigashi, H.; Hakuraku, Y.; Onabe, K.; Okada, M.; Kashima, N.; Nagaya, S. {110} <112> and {110} <110> textured Ag tapes for biaxially oriented $YBa_2Cu_3O_7$ coated conductors. *Phys. C Supercond.* **2002**, *378–381*, 927–931. [CrossRef]
14. Suo, H.; Genoud, J.Y.; Schindl, M.; Walker, E.; Tybell, T.; Cléton, F.; Zhou, M.; Flükiger, R. Stable {110} ⟨ 112⟩ textured Ag ribbons for biaxially-aligned $YBa_2Cu_3O_{7-\delta}$ coated tapes. *Supercond. Sci. Technol.* **2000**, *13*, 912–919. [CrossRef]
15. Goyal, A.; Norton, D.P.; Christen, D.K.; Specht, E.D.; Paranthaman, M.; Kroeger, D.M.; Budai, J.D.; He, Q.; List, F.A.; Feenstra, R. Epitaxial superconductors on rolling-assisted biaxially-textured substrates (RABiTS): A route towards high critical current density wire. *Appl. Supercond* **1996**, *4*, 403–427. [CrossRef]
16. Zhang, Z.-R.; Sekine, K. Development of single sharp {011} <211> recrystallization texture in polycrystalline silver by severe plastic deformation at room temperature. *Mater. Sci. Eng. A* **2006**, *423*, 243–246. [CrossRef]
17. Cheng, C.; Feng, Y.; Chen, Z.; Li, H.E.; Wang, X.; Wang, Q. Effect of annealing temperature on microstructure, texture and tensile properties of TA32 sheet. *Mater. Sci. Eng. A* **2021**, *826*, 141971. [CrossRef]
18. Li, X.H.; Yan, H.; Chen, R.S. Microstructure, texture and mechanical properties of Y_2O_{3P}/ZG21 composites after rolling and subsequent annealing. *J. Alloys Compd.* **2021**, *889*, 161683. [CrossRef]
19. Liang, X.; Wu, Q.; Li, H.; Wang, R.; Kang, L.; Liu, B.; Wang, L. Static recrystallization and texture evolution of cold-rolled powder metallurgy CoCrFeNiN0.07 high-entropy alloy. *J. Alloys Compd.* **2021**, *862*, 158602. [CrossRef]
20. Jandaghi, M.R.; Pouraliakbar, H.; Shiran, M.K.G.; Khalaj, G.; Shirazi, M. On the effect of non-isothermal annealing and multi-directional forging on the microstructural evolutions and correlated mechanical and electrical characteristics of hot-deformed Al-Mg alloy. *Mater. Sci. Eng. A* **2016**, *657*, 431–440. [CrossRef]
21. Sun, B.; Shen, T. Probing the Deformation Mechanisms of Nanocrystalline Silver by In-Situ Tension and Synchrotron X-ray Diffraction. *Metals* **2020**, *10*, 1635. [CrossRef]
22. Wang, Y.Q.; Wen, M.; Guo, J.M.; Xiao, Z.; Gan, J.Z.; Wang, C.J.; Tan, Z.L.; Guan, W.M. EBSD Study on the Recrystallization Behavior of Ni-5Pt Alloy. *Rare Met. Mater. Eng.* **2022**, *51*, 127–133.
23. Conrad, H.; Jung, K. Effect of grain size from millimeters to nanometers on the flow stress and deformation kinetics of Ag. *Mater. Sci. Eng. A* **2005**, *391*, 272–284. [CrossRef]
24. Paul, H.; Driver, J.H.; Maurice, C.; Piątkowski, A. Recrystallization mechanisms of low stacking fault energy metals as characterized on model silver single crystals. *Acta Mater.* **2007**, *55*, 833–847. [CrossRef]